Heterogeneous & Homogeneous & Bio- & Nano-
CHEMCATCHEM
CATALYSIS

Accepted Article

Title: Relationship between acid-base properties and the activity of ZrO2 catalysts for the Cannizzaro reaction of pyruvaldehyde to lactic acid

Authors: Elise M. Albuquerque, Luiz E.P. Borges, Marco A. Fraga, and Carsten Sievers

To be cited as: *ChemCatChem* 10.1002/cctc.201700305

Link to VoR: http://dx.doi.org/10.1002/cctc.201700305

A Journal of
ChemPubSoc Europe

WILEY-VCH

www.chemcatchem.org

Relationship between acid-base properties and the activity of ZrO_2–based catalysts for the Cannizzaro reaction of pyruvaldehyde to lactic acid

Elise M. Albuquerque,[a,b,c] Luiz E. P. Borges,[b] Marco A. Fraga*[a,b] and Carsten Sievers*[c]

Abstract: The Cannizzaro reaction of pyruvaldehyde to lactic acid is investigated in a flow reactor using ZrO_2 catalysts with different structures and acid-base properties. The results show that the difference in crystalline structures of two ZrO_2 polymorphs strongly affects the conversion of pyruvaldehyde. The monoclinic phase of zirconia is the most active for this reaction. A good correlation is observed between the reaction rate and the concentration of Lewis acid sites of sufficient strength, showing that these sites play a major role in the reaction. A reaction mechanism is proposed involving coordinatively unsaturated Zr^{4+} cations as sites for activating pyruvaldehyde molecules, while Zr^{4+}-O^{2-} pairs generate terminal OH groups through water dissociation.

Introduction

The world energy supply is still dominated by fossil resources (such as coal, oil and natural gas). The continued use of these resources leads to severe environmental problems like global warming, escalating the necessity to develop new technologies for generating energy and chemicals from renewable resources.[1] Biofuels have attracted strong interest as means of sustainable fuel production and providing value from agricultural residues.[1] Since their combustion characteristics are similar, they can replace the fossil fuels, like gasoline and diesel, with limited modification to the engines.[2]

In particular, biodiesel gained worldwide attention, since it offers advantages like a sustainable production chain, low toxicity, biodegradability, so that it can be considered less polluting than conventional petrodiesel.[3] However, the production of glycerol as a by-product is inevitable and accounts for about 10% of the volume of biodiesel produced.[4] The amount of glycerol produced in this process exceeds the demand for its conventional uses by far.

Many efforts have thus been made to develop chemical process technologies to convert glycerol into value-added products through oxidation,[5] dehydrogenation,[6] etherification,[7] acetalization[8] and condensation.[9]

As a three-carbon backbone molecule, glycerol could be converted to lactic acid, an important product with a gradually increasing demand due to its many end-use applications in food and beverages, personal care, pharmaceuticals and plastic manufacturing.[10] Lately, the production of biodegradable poly(lactic acid), PLA, has become a major driving force for the growth of the global lactic acid market.[11]

Hydrothermal conversion of glycerol into lactic acid through homogeneous processes has been reported, but it only proceeds in the presence of large amounts of inorganic hydroxides,[12] like NaOH and KOH, which are not recycled or recovered. This matter impacts the environmental footprint of the process and increases production costs.

Lactic acid can also be obtained from glycerol over heterogeneous catalysts. The direct reaction was reported over mono-metallic and bimetallic catalysts based on Au, Pd and Pt in the presence of NaOH.[13] High lactic acid selectivity (85%) has been reached,[13] but the use of undesirable inorganic hydroxides is still necessary.

Alternative approaches use cascade reactions to produce lactic acid from glycerol. For example, glycerol may be initially dehydrated to hydroxyacetone[14] on solid acid catalyst and then this ketone can be converted into lactic acid by oxidation/intramolecular rearrangement, which may occur in alkaline medium[15] or on solid basic catalysts, such as hydrotalcites and hydrotalcites derived mixed oxides.[16] Glycerol can also be converted to 1,2-propanediol by hydrogenolysis,[17] which can be oxidized to lactic acid.[18] Selective oxidation (dehydrogenation) of glycerol to dihydroxyacetone[19] followed by dehydration/intramolecular rearrangement[19b,20] is also a feasible process.

Independently of the process and the reaction pathway, pyruvaldehyde is a key intermediate towards lactic acid in most reports.[13,15-16,18,19b] Some researchers even showed that more selective lactic acid production is accomplished when glycerol is initially and directly converted to pyruvaldehyde instead of dihydroxyacetone and then rearranged to lactic acid.[19b] However, despite such advantages of a two-step process with pyruvaldehyde as the only isolated chemical intermediate, there are just a few studies focused on its rearrangement into lactic acid.[21]

[a] Dr. E. M. Albuquerque, Dr. M. A. Fraga
Divisão de Catálise e Processos Químicos
Instituto Nacional de Tecnologia/MCTIC
Av. Venezuela, 82/518, Saúde, Rio de Janeiro/RJ 20081-312, Brazil
E-mail: marco.fraga@int.gov.br

[b] Dr. E. M. Albuquerque, Prof. L. E. P. Borges, Dr. M. A. Fraga
Seção de Química
Instituto Militar de Engenharia
Praça Gen Tibúrcio, 80, Praia Vermelha, Urca, Rio de Janeiro/RJ 22290-270, Brazil

[c] Dr. E. M. Albuquerque, Prof. C. Sievers
School of Chemical & Biomolecular Engineering
Georgia Institute of Technology
311 Ferst Dr. NW., Atlanta, Georgia 30332-0100, United States
E-mail: carsten.sievers@chbe.gatech.edu

Supporting information for this article is given via a link at the end of the document.

Pyruvaldehyde conversion to lactic acid occurs via its intramolecular disproportionation, also known as Cannizzaro reaction (Scheme 1). It is well reckoned that the rearrangement of α-keto aldehydes leads to α-hydroxy carboxylic acids in strong basic medium.[22] Such transformation is also possible in the presence of acids. However, Brönsted acids (HCl, H_2SO_4) are not as effective as Lewis acids.[21b] Koito et al. reported that only water-tolerant homogeneous Lewis acids, such as scandium, yttrium and ytterbium triflates, achieved high catalytic activity in the intramolecular Cannizzaro disproportionation with lactic acid yields higher than 94%.[21b] As mentioned above, the corrosiveness and toxicity of alkaline or acidic solutions is cause for environmental concerns. Therefore, the design of a greener heterogeneously-catalyzed process is imperative to allow for the valorization of glycerol via lactic acid production in a truly sustainable way. However, various challenges have to be overcome to understand and control the surface chemistry and stability of heterogeneous catalysts for this process.[23]

A few recent studies used batch reactors to provide some insight into the conversion of pyruvaldehyde to lactic acid over solid catalysts such as MgO,[24] ZrO_2[24] and Nb_2O_5.[21b] Acidic Nb_2O_5 was found to be quite efficient even with a low density of water-tolerant Lewis acid sites.[21b] Its strong acidity, however, promoted the formation of numerous polymerized species. Amphoteric ZrO_2 provided higher yield of lactic acid than highly basic MgO in neutral or weakly acidic/basic aqueous medium, whose pH was cautiously adjusted for the reaction.[24]

In this contribution, the Cannizzaro reaction of pyruvaldehyde over zirconium oxide-based catalysts is investigated using continuous flow reactor setup. These catalysts were chosen due to their amphoteric properties and hydrothermal stability. Furthermore, polymorphic structures of ZrO_2 and their ability to embed foreign cations allow for tailoring surface properties to unveil the role of acid and basic surface sites on the reaction. The reactions in this study were performed without any addition of alkaline or acidic solutions.

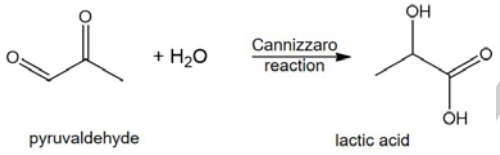

Scheme 1. Reaction scheme for the Cannizzaro reaction of pyruvaldehyde to lactic acid.

Results

Catalyst characterization

The composition of the doped catalyst is summarized in Table 1. All catalysts were characterized by XRD and Raman spectroscopy to determine their structures.

Pure zirconia samples exhibited diffraction peaks characteristic of either monoclinic (COD 9007485) or tetragonal (COD 1525705) crystalline structures (Figure S1a). The doped zirconias, Y-ZrO_2 and La-ZrO_2, showed diffraction patterns similar to that of a tetragonal phase. However, a small shift to lower Bragg angles can be noticed, which is made clear by enlarging the angular region corresponding to the *hkl* line (111) (Figure S1b). Despite these structural distortions all diffractions matched those expected for a tetragonal structure, revealing that either no isolated crystalline Y_2O_3 or La_2O_3 phases were present or that they were below the XRD detection limit.

Table 1. Surface area (S_{BET}), pore volume (V_p), average diameter (d_p) and the amount of dopant oxide (DO) of all zirconia catalysts.

Catalyst	S_{BET} ($m^2.g^{-1}$)	V_p ($cm^3.g^{-1}$)	d_p (Å)	DO (%)
m-ZrO_2	103	0.304	90	-
t-ZrO_2	129	0.165	46	-
Y-ZrO_2	102	0.163	49	5
La-ZrO_2	94	0.209	72	8
TiO_2-ZrO_2	49	0.290	111	35

On the other hand, TiO_2-ZrO_2 gave a more complex diffractogram (Figure S1a and S1c), containing peaks associated with both monoclinic and tetragonal phases of zirconia, and also the anatase structure of TiO_2 (COD 9009086).

The Raman spectrum of commercial *m*-ZrO_2 (space group $P2_{1/c}$) exhibited bands at 101, 177, 189, 221, 307, 332, 346, 380, 476, 501, 535, 557, 616 and 632 cm^{-1} corresponding to its active vibrational modes ($9A_g+9B_g$ symmetry) (Figure S2).[25] For *t*-ZrO_2 (space group $P4_{2/nmc}$), five bands were recorded at 150, 274, 317, 461 and 646 cm^{-1}, which are related to its Raman active vibrational modes ($A_{1g}+2B_{1g}+3E_g$).[25-26]

The spectra of Y-ZrO_2 and La-ZrO_2 doped zirconias were comparable to that of *t*-ZrO_2, exhibiting the same typical Raman bands of a tetragonal lattice. No Raman shifts could be associated with any isolated crystalline or amorphous Y_2O_3 or La_2O_3 phases. However, in case of TiO_2-ZrO_2, the Raman spectrum was totally different from the others; five bands were observed at 150, 201, 398, 519 and 640 cm^{-1}, which are well related to the six vibrational modes $A_{1g}+2B_{1g}+3E_g$ of titania anatase phase (space group $I4_{1/amd}$).[27] The spectrum also contained a small band at 484 cm^{-1} that can be associated with the monoclinic phase of zirconia.

The porosity and surface area of the catalysts were assessed by N_2 physisorption (Table 1, Figure S3a). All oxides presented the same type IVa isotherm, according to IUPAC classification,[28] indicating the presence of mesopores. All catalysts, except for TiO_2-ZrO_2, presented high surface areas above 90 $m^2.g^{-1}$ and average pore diameters above 45 Å (Table 1). The pore size distributions obtained from Barret-Joyner-Halenda (BJH) method had a reasonably sharp peak centered around 40 Å for the catalysts with a tetragonal structure and around 70-80 Å for the

other two samples that are dominated by the monoclinic zirconia phase (Figure S3b).

The concentration and strength of base sites was probed by TPD of CO_2 (Figure 1, Table 2). The catalysts CO_2 desorption profiles were similar with an intense desorption peak below 200 °C and a long tail extending to temperatures as high as 500 °C. Such traces indicate that the samples possess a wide distribution of surface base sites in terms of their strength. While all samples contained base sites with a range of different strengths, the relative abundance of weak and strong sites varied between the samples. The *m*-ZrO_2 catalyst possessed a higher concentration of base sites than its polymorph *t*-ZrO_2. Doping zirconia with yttrium and lanthanum increased the basicity of the *t*-ZrO_2. Lastly, TiO_2-ZrO_2 showed the lowest concentration of base site.

Table 2. Concentration of weak, medium and strong base and acid sites of all ZrO_2 catalysts as determined by CO_2 and NH_3 temperature-programmed desorption analysis.

Catalyst	Base sites ($\mu molCO_2.g^{-1}$)				Acid sites ($\mu molNH_3.g^{-1}$)			
	Weak[a]	Medium[b]	Strong[c]	Total	Weak[d]	Medium[e]	Strong[f]	Total
m-ZrO_2	113	79	54	246	56	68	63	187
t-ZrO_2	53	26	10	89	54	54	34	142
Y-ZrO_2	101	86	65	252	38	57	31	126
La-ZrO_2	75	55	67	197	76	54	13	143
TiO_2-ZrO_2	36	26	9	71	55	66	61	181

[a] desorption temperatures up to 170 °C. [b] desorption temperatures between 150-300 °C. [c] desorption temperatures above 300 °C. [d] desorption temperatures up to 200 °C. [e] desorption temperatures between 200-400 °C. [f] desorption temperatures above 400°C.

The characterization of acid sites by temperature-programmed desorption of NH_3 provided traces with three distinct desorption peaks for all catalysts (Figure 2). The most intense peaks were recorded below 250 °C, but the strength distribution of the acid sites was much wider with a shoulder extending to much higher temperatures. The *m*-ZrO_2 catalyst had the highest density of acid sites, whereas all catalysts with tetragonal structure presented lower acid site concentrations (Table 2). The strength distribution of the acid sites was analyzed based on mathematical deconvolution of the TPD traces. The *m*-ZrO_2 and TiO_2-ZrO_2 catalysts had similar concentrations of each type of acid sites (weak, medium and strong sites). *t*-ZrO_2 contains mostly weak and medium acid sites, while Y-ZrO_2 has a higher concentration of medium site, and La-ZrO_2 showed a higher density of weak acid sites and a lower concentration of strong sites.

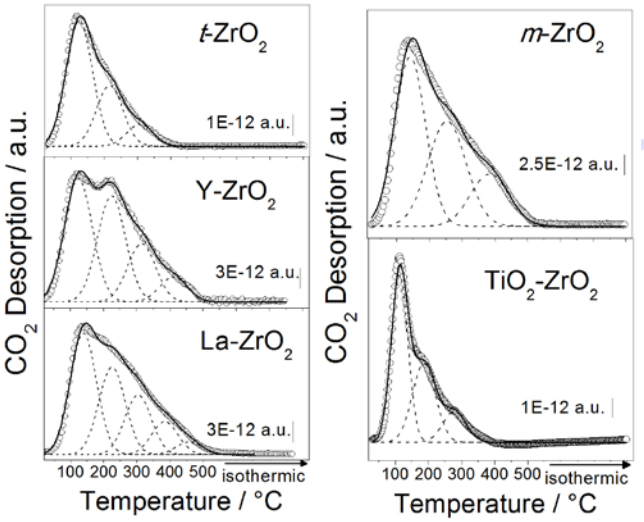

Figure 1. CO_2 temperature-programmed desorption profiles of ZrO_2-based catalysts.

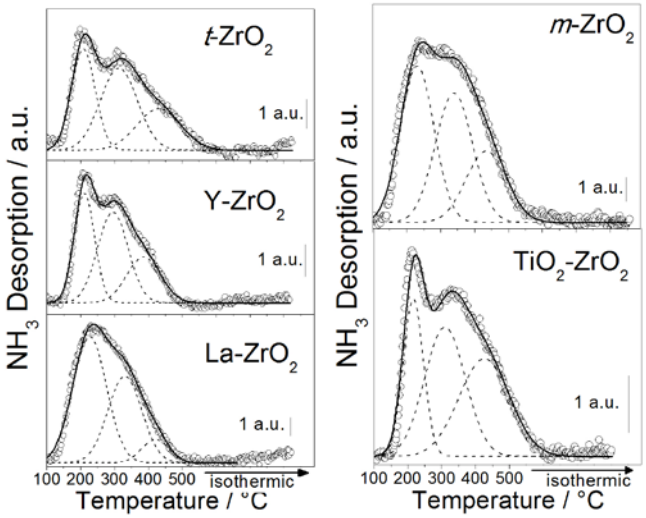

Figure 2. NH_3 temperature-programmed desorption profiles of ZrO_2–based catalysts.

Catalytic reactivity tests

In order to compare the intrinsic activity of all catalysts, the effect of mass transfer limitations were probed for the most active catalyst, *m*-ZrO_2. No perceivable variation in pyruvaldehyde conversion was found when the flow rate of the feed was varied at constant space time, allowing for the conclusion that the reaction was not limited by external mass transfer (Figure 3a). Likewise, any pore diffusion limitations were found to be irrelevant, since a variation of the catalyst particle size did not result in significant changes in conversion (Figure 3b). Based on these preliminary experiments, all other reactions were performed with a particle size of 53-63 µm, a flow rate of 0.2 mL.min^{-1}, and a space time of 3.5 min to ensure that all measurements were carried out in the microkinetic regime.

The performance of both zirconia polymorphs was initially evaluated. As expected, pyruvaldehyde conversion increased with increasing temperature (Figure 4). Simultaneously, the yield of lactic acid increased, but its selectivity did not change significantly throughout the reaction (Figure 4d) between 100 and 130 °C. Figure 4 also shows the results of reaction without any catalyst. Only traces of lactic acid were formed, but pyruvaldehyde was degraded to other products when the temperature increased.

A clear difference between the behaviors of the two polymorphic catalysts is seen though. While pyruvaldehyde conversion reached 75% over *m*-ZrO_2 at 130 °C (Table 3), only 36% conversion were accomplished over *t*-ZrO_2 (Table 3). The conversion over *m*-ZrO_2 increased consistently with increasing reaction temperature up to 180 °C, ultimately reaching about 90% (Figure 5a). However, the lactic acid selectivity began dropping above 160 °C, as a consequence, lactic acid yield dropped as well, suggesting that an increasing fraction of pyruvaldehyde was converted via side reactions. When the temperature was decreased back to 140 °C, the conversion did not reach the same level as before (Figure 5a). This indicates that at least some of the side reactions led to deactivation of the catalyst, presumably by formation of carbonaceous deposits, which could occur by condensation reactions of pyruvaldehyde and/or lactic acid at high temperatures (>160 °C).[21b] As a matter of fact, the color of the catalyst turned to dark brown (Figure 5b) after reaction at such temperatures, providing further evidence for the deposition of carbonaceous compounds on the catalyst. TGA analysis of spent catalysts showed 10.0% of weight loss at temperatures above 200 °C (Figure S4), which is another sign for the presence of carbonaceous deposits.

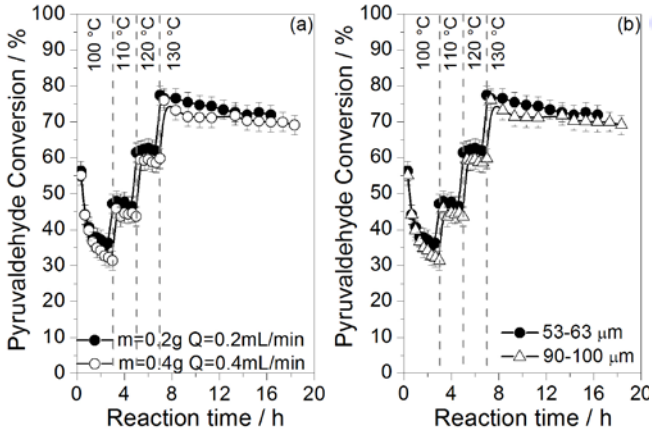

Figure 3. Pyruvaldehyde conversion at 100-130 °C for tests of (a) external mass transfer – different catalysts weight at constant space time (τ = 3.5 min) and (b) internal mass transfer with different particle sizes at constant space time (τ = 3.5 min) over *m*-ZrO_2 catalyst.

Table 3. Pyruvaldehyde conversion (X_P), lactic acid selectivity (S_{LA}) and yield (Y_{LA}), reaction rate ($-r_A$) at 130 °C and activation energy (Ea) determined for all ZrO_2 catalysts.

Catalyst	X_P (%)	S_{LA} (%)	Y_{LA} (%)	$-r_A$ (mmol.g^{-1}.min^{-1})	Ea (kJ.mol^{-1})
m-ZrO_2	75	75	56	93.2	47.7
t-ZrO_2	36	79	29	71.8	41.8
Y-ZrO_2	35	72	25	71.5	49.6
La-ZrO_2	36	69	25	72.0	40.0
TiO_2-ZrO_2	56	81	45	85.0	40.5

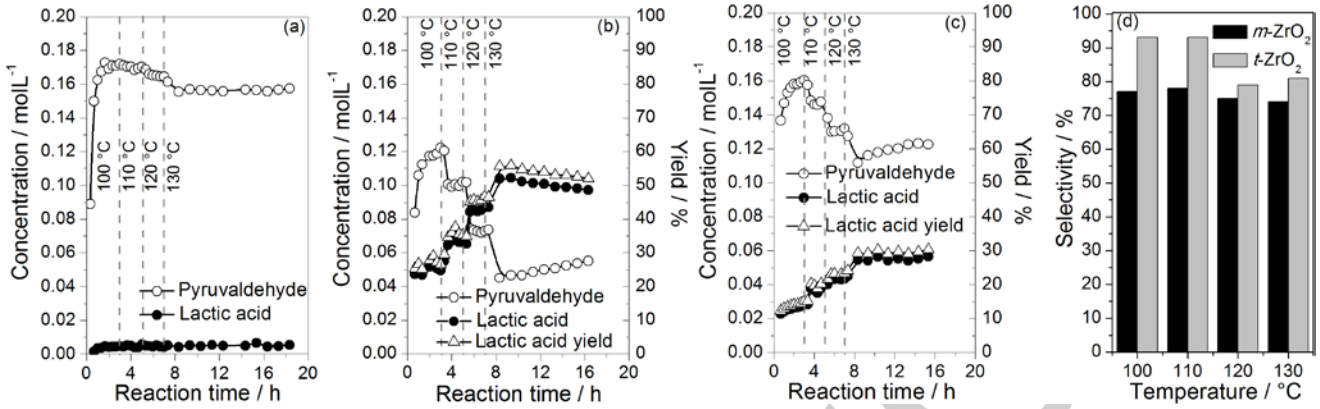

Figure 4. Pyruvaldehyde and lactic acid concentration and yield obtained at 100-130 °C without catalyst (a), over *m*-ZrO_2 (b) and *t*-ZrO_2 (c) polymorphic catalysts and (d) lactic acid selectivity for both catalysts at τ = 3.5 min; flow rate = 0.2 mL.min^{-1} and particle size = 53-63 µm.

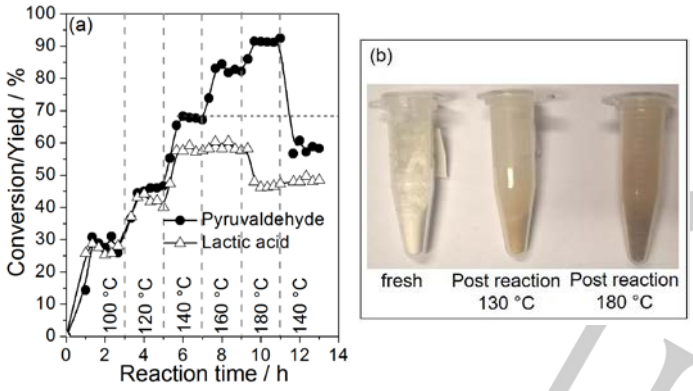

Figure 5. Pyruvaldehyde conversion at 100-180 °C on *m*-ZrO_2 (a) and catalyst color change after reaction (b) at τ = 3.5 min; flow rate = 0.2 mL.min^{-1} and particle size = 53-63 µm.

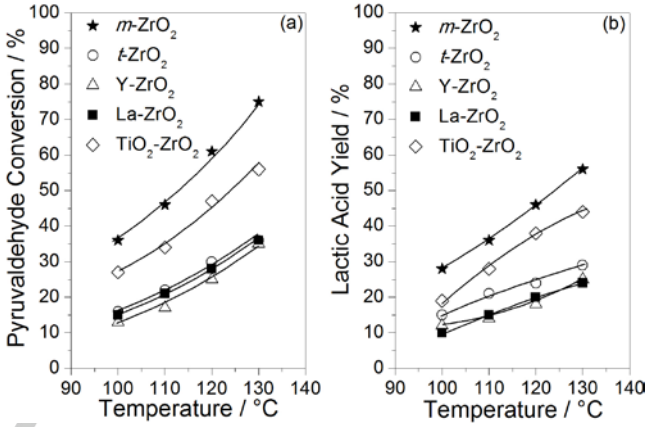

Figure 6. Pyruvaldehyde conversion (a) and lactic acid yield (b) obtained at 100-130 °C over ZrO_2-based catalysts at τ = 3.5 min; flow rate = 0.2 mL.min^{-1} and particle size = 53-63 µm.

The doped ZrO_2 catalysts with a tetragonal structure were less active, exhibiting similar pyruvaldehyde conversion and lactic acid yield to that over pure *t*-ZrO_2 (Figure 6). For TiO_2-ZrO_2, an intermediate behavior was observed (Table 3). Independently of the catalyst used, lactic acid selectivity was always fairly constant, ranging between 70 to 80% between 100-130 °C. The increased yield (Figure 6b) is a reflex of the higher conversion. The apparent activation energies for all catalysts were determined to be 40–50 kJ·mol^{-1} based on an Arrhenius plot (Figure S5) (Table 3).

Discussion

Physico-chemical Characteristics of Catalysts

Zirconium oxide is an attractive catalyst for aqueous-phase processing due to its amphoteric character, combining acid and base properties.[29] Depending on the reaction medium and the nature of reactants, either type of sites can be dominant. Moreover, the availability of different polymorphs and the structural flexibility to accommodate foreign cations as solid solutions allow for tuning its surface properties. XRD analyses confirmed the monoclinic and tetragonal ZrO_2 polymorphic structures of the materials used in this work. It also showed that the doped samples Y-ZrO_2 and La-ZrO_2 consist of a distorted tetragonal phase characterized by a shift of the *hkl* line (111) to lower Bragg angles. This shift suggests that their structural distortion arises from the insertion of dopant elements (yttrium or lanthanum) with larger ionic radii into zirconia lattice, and therefore, the material can be described as ZrO_2-based solid

solutions. Raman spectra corroborated these conclusions and additionally revealed that no significant amounts of amorphous isolated phases are present in these catalysts. This indicates that the dopants are quantitatively incorporated into the ZrO_2 framework. It also explains the formation of a stable tetragonal structure in these doped samples at moderate calcination temperatures, whereas it is well-known that pure *t*-ZrO_2 can only be formed by calcination at very high temperatures (>1000 °C).[30]

The commercial TiO_2-ZrO_2 catalyst had a more complex structure. The X-ray diffractogram indicated that it contained a mixture of a monoclinic and tetragonal zirconia phases and an anatase TiO_2 phase.

One should bear in mind that these zirconia polymorphs present distinct atom conformation. In the monoclinic crystal phase the Zr^{4+} cations are heptacoordinated, and the O^{2-} anion is tri- or tetracoordinated. On the other hand, in the tetragonal structure, Zr^{4+} cations are octacoordinated, and the O^{2-} is tetracoordinated.[29c,31] Such different coordinations and structural arrangements will generate different types of coordinatively unsaturated surface sites and consequently lead to quite distinct acid-base surface properties. Additionally, the distribution of hydroxyl groups is also affected by the different structures, since these OH groups will be coordinated to those unsaturated centers on the surface. We previously reported that these commerical *m*-ZrO_2 presented both mono and multi-coordinated OH groups, whereas *t*-ZrO_2 only contains multiply coordinated OH groups.[31]

Quantitative TPD-CO_2 results clearly showed that the *m*-ZrO_2 polymorph had the highest basicity, with a concentration of base sites almost three times as high as that of its tetragonal polymorphic counterpart (Table 2). Interestingly, introduction of trivalent yttrium and lanthanum cations into the tetragonal framework of zirconia significantly increased its basicity, rendering solids as basic as *m*-ZrO_2. Furthermore, the solid solutions contained a higher fraction of medium and strong base sites compared to pure *t*-zirconia (Table 2). TiO_2-ZrO_2 presented the lowest concentration of base sites, with weak and medium base sites accounting for almost 90% of the total amount of sites. It is worth mentioning that total basicity of this catalyst cannot be rationalized in a simple way, since it certainly arises from different contributions coming from all three crystalline phases composing the TiO_2-ZrO_2 catalyst as identified by XRD.

The acidity of the catalysts exhibited a different trend, particularly considering the two polymorphs catalysts. The *m*-ZrO_2 presented the highest concentration of acid sites, around twice that of the pure *t*-ZrO_2 catalyst. However, no substantial effects were observed by adding Y or La into the crystal lattice of zirconia (Table 2).

Taking into account that the coordinatively unsaturated cations are the ones credited for the Lewis acidity, it is conceivable the occurrence of different surface Zr^{4+} sites induced by the different types of O^{2-} anions on both polymorphic structures. It has indeed been reported that those two different O^{2-} anions (trigonally and tetrahedrally coordinated) on the surface of monoclinic zirconia engender two discrete surface sites of Zr^{4+} in *m*-ZrO_2, while the tetracoordinated O^{2-} species induce only one type of Zr^{4+} cation in *t*-ZrO_2.[29c, 32] The existence of such distinct Zr^{4+} centers designing two types of Lewis-acidic sites has been also shown by experimental spectroscopic studies reported elsewhere.[29a,33] This distinct cation environment may be responsible for such higher acidity of *m*-ZrO_2 catalyst observed in this study.

Catalytic reactivity tests

All zirconia-based catalysts were initially tested in a continuous flow fixed-bed reactor covering a range of temperatures. As expected, the conversion increased with increasing reaction temperature, but the yield of lactic acid was affected negatively at the highest temperatures, since the selectivity decreased above 160 °C (Figure 5a). Catalyst deactivation was evidenced by reduced conversion, while the change in color of the catalyst (Figure 5b) and the TGA profile (Figure S4) of the spent catalyst pointed at the formation of carbonaceous deposits as the likely reason. It is suggested that these species are formed in condensation reactions of the reagent and/or products. Some authors have indeed reported the formation of complex polymerized species by intermolecular reactions of pyruvaldehyde on $Nb_2O_5 \cdot nH_2O$ as assessed by MALDI-TOF mass spectrometry at 140 °C.[21b] Based on these experimental findings, we limited our kinetic study to temperatures up to 130 °C, so that reliable conclusions regarding the performance of different ZrO_2-based catalysts can be derived.

To further assure the validity of conclusions regarding the microkinetic performance of the catalysts, it was established that the conversion over the most active catalyst, *m*-ZrO_2, is not affected by internal or external mass transfer limitations. The lactic acid selectivity was fairly constant with respect to temperature (up to 130 °C) and similar between all catalysts, though. It is consistent with the very similar activation energies found for lactic acid formation and indicates that the temperature cannot be used as a variable to control selectivity.

It is generally known that intramolecular disproportionation of pyruvaldehyde can occur in basic media.[15,34] Based on this knowledge and the high concentration of base sites on *m*-ZrO_2, one could expect this catalyst to show the highest activity.

Despite the superior activity performance of *m*-ZrO_2 catalyst, any attempt to consistently correlate this property with the reaction kinetics over all catalysts failed (Figure 7a), suggesting that the base sites are not the only sites involved in the conversion of pyruvaldehyde over these catalysts.

A plausible correlation of the catalytic behavior can be obtained with the acid site concentration of the catalysts (Figure 7b). Specifically, the activity increased linearly with increasing total concentration of acid sites. Therefore, it is suggested that the conversion of pyruvaldehyde into lactic acid is predominantly catalyzed by the Lewis acid sites on all the zirconia-based samples. This is in line with the observation of similar activation energies for all samples, which corroborates that reaction follows the same mechanism over all catalysts studied here. In fact, the Cannizzaro reaction has been reported to be catalyzed in the presence of homogeneous Lewis acids like $AlCl_3$.[21b,35] In an attempt to provide further insight into the strength requirements for acid sites the concentrations of weak (Figure

7c), medium (Figure 7d) and strong (Figure 7e) acid sites were compared to the rate of reaction. As can be observed, the weak acid sites are not playing any role in the reaction while the medium and strong acid sites seem to be the active ones for the Cannizzaro reaction. However, the correlation is more satisfactorily described for the acid sites with medium strength (Figure 7d), since it can be easily extrapolated to zero.

We propose that the correlation between catalytic activity and the concentration of medium Lewis acid sites exists because the conversion of pyruvaldehyde starts by adsorption of the reactant to a coordinatively unsaturated Zr^{4+} ion acting as a Lewis acid site through both carbonyl groups (keto and aldehyde groups) forming a five membered ring, as presented in Scheme 2. The results indicate that this interaction between the pyruvaldehyde molecule and Zr^{4+} needs a minimum strength for the reaction to occur. Deviations observed by correlating the strong acid sites suggest that they might bind the intermediate species too strongly for optimal activity.

After such activation of the aldehyde group, a water molecule must be added to allow the rearrangement to lactic acid. We proposed that it occurs via dissociation of water from the reaction medium on coordinatively unsaturated Zr^{4+}-O^{2-} pairs on the surface of the catalyst (Scheme 2). The isolated singly coordinated OH groups formed on the Zr^{4+} can be transferred to the adsorbed pyruvaldehyde molecules through a nucleophilic attack, followed by a hydride shift to form lactic acid. The proposed bifunctional acid-base reaction mechanism also explains the difference in the performance of both ZrO_2 polymophs. It is well-known that isolated singly coordinated OH groups are predominantly found in the monoclinic catalyst while *t*-ZrO_2 does not possess these terminal OH groups.[29a,31-32] The cooperativity between sufficiently strong Lewis acid sites and terminal OH groups could be the reason for the high activity of *m*-ZrO_2 catalyst.

The hydroxyls consumed upon intramolecular Cannizzaro disproportionation are assumed to be continuously replaced by water dissociation on catalyst surface. Involvement of surface hydroxyls from heterogeneous catalysts is indeed quite common in solid-catalyzed reactions and the geometry of such OH groups are usually the key issues.[36]

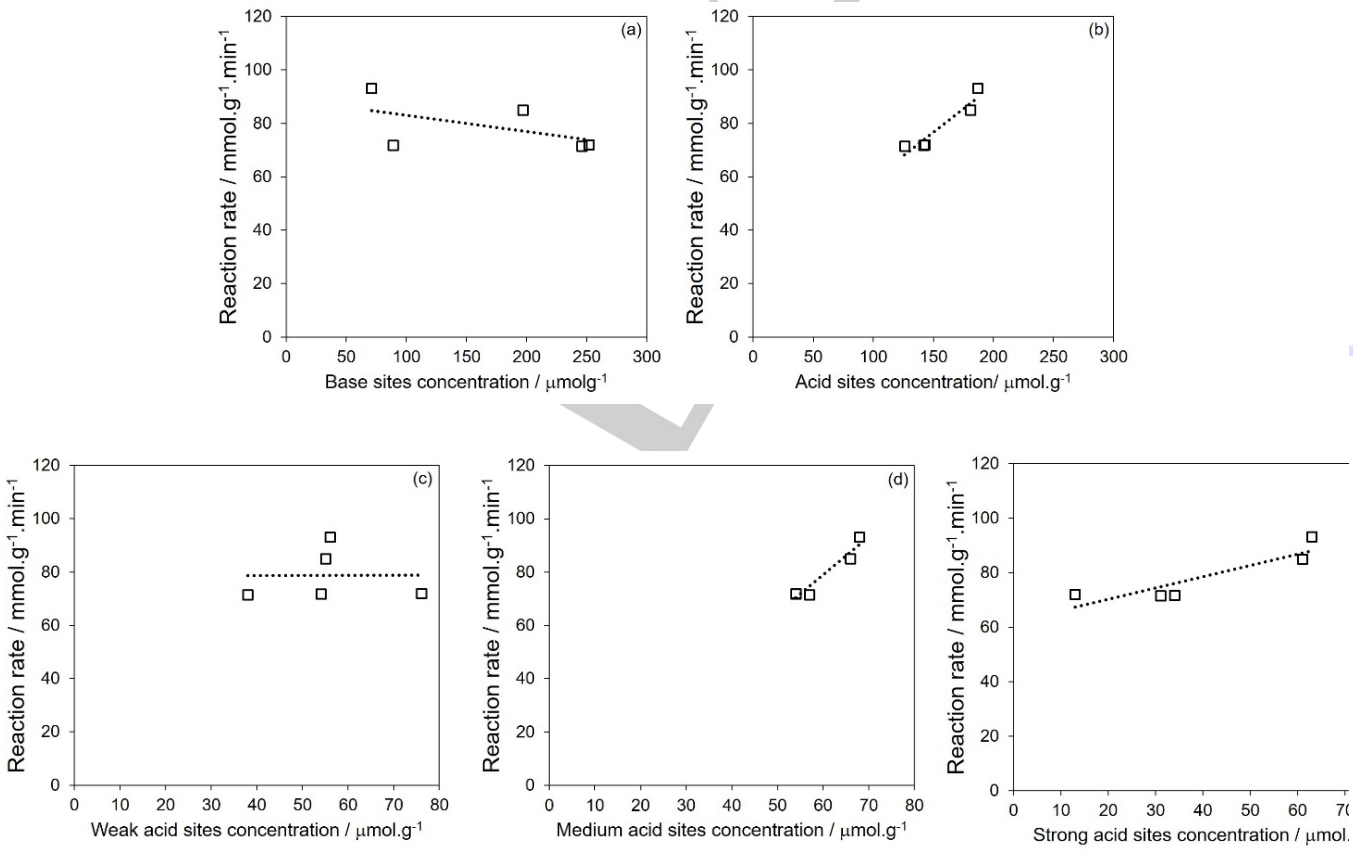

Figure 7. Correlation between reaction rate and concentration of base (a), total acid sites (b), weak acid sites (c), medium acid sites (d) and strong acid sites (e)

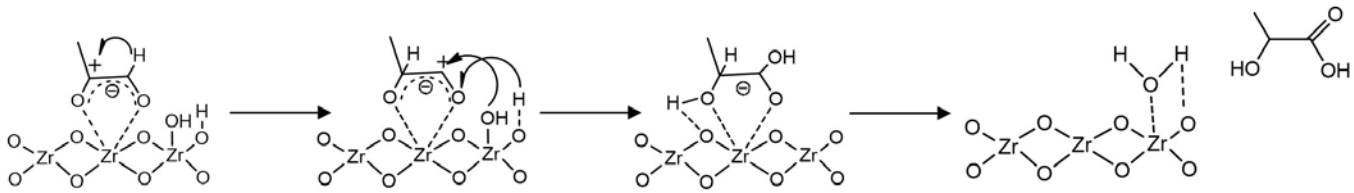

Scheme 2. Proposed reaction mechanism of pyruvaldehyde Cannizzaro reaction on ZrO_2 surface.

Similar proposals have very recently been presented for lactic acid formation from xylose retro-aldol condensation followed by intramolecular Cannizzaro disproportionation on both ZrO_2 and MgO catalysts.[24] However, the authors did not provide any information regarding the crystal structure of the ZrO_2 catalyst on the reaction mechanism of the Cannizzaro reaction of pyruvaldehyde to lactic acid, which we show herein to be crucial for the performance of this catalyst. Besides considering the reaction steps on the catalyst surface, a possible contribution from OH^- nucleophiles and H_3O^+ hydronium species generated by self-dissociation of water has to be discussed. The results from our blank experiment (Figure 4a) indeed suggest that such species may play a role in lactic acid formation since it was detected after all. However, it is clear that is not kinetically favoured, highlighting the role of the catalyst in providing all intermediate species on its coordinatively unsaturated sites.

Taking into account this discussion and the data reported in literature regarding the use of alkaline and earth alkaline hydroxides, it seems that the Cannizzaro reaction in the presence of a homogenous or heterogeneous catalysts adopt the same mechanism. All in all, the Lewis acid sites (Na^+, K^+ or Zr^{4+}) act as the anchoring centers for the aldehyde molecule, and the OH groups could come from dissociation of a homogeneous catalysts (e.g. NaOH) or mobile surface hydroxyl groups on heterogeneous catalysts that are replenished by water dissociation. The information obtained herein provides us a better understanding of the catalyst surface properties on this reaction, contributing to design a more efficient catalyst.

Conclusions

The results presented herein show that it is possible to convert pyruvaldehyde into lactic acid using solid catalysts without any pH control by the addition of homogeneous alkaline or acid solutions. Zirconium oxide holding a monoclinic crystalline structure was found to be a more active catalyst than its tetragonal counterpart. Lattice doping with trivalent yttrium or lanthanum cations altered the acid-base properties but did not improve the catalytic activity of tetragonal-structured catalysts. Amphoteric zirconia oxides showed that the intramolecular Cannizzaro reaction occurs on solid acid sites via a bifunctional acid-base mechanism involving coordinatively unsaturated Zr^{4+} cations and coordinatively unsaturated Zr^{4+}-O^{2-} pairs responsible for generating terminal OH groups through water dissociation.

Experimental Section

Materials

Commercial ZrO_2 oxides were provided by Saint Gobain Norpro. The different oxides used in this work were monoclinic (*m*-ZrO_2) and tetragonal (*t*-ZrO_2) zirconias, zirconia doped with yttrium (Y-ZrO_2) and lanthanum (La-ZrO_2), and a titania-zirconia mixed oxide (TiO_2-ZrO_2). Sulfuric acid (95-98%) from Sigma-Aldrich, pyruvaldehyde (35-45 %w/w aqueous solution) and lactic acid (85-90%) from Alfa Aesar, and pyruvic acid (98%) from Acros were used without any purification.

Catalyst characterization

X-ray diffraction analyses (XRD) were performed on a Bruker D8 Advance with DaVinci design diffractometer equipped with a Lynxeye position sensitive detector. Diffractograms were collected using CuKα radiation at a rate of 0.02° per step between 20° and 90°. Samples were analyzed as powders without any pretreatment. The software DiffracEva V2.0 from Bruker was used to identify crystalline phases.

Raman spectra were collected on a Horiba (Jobin Yvon) HR800 UV spectrometer with a thermal conductivity detector at -70 °C, using a He-Ne laser at 632.8 nm. The data were collected between 100 and 800 nm. All samples were analyzed as powder without any pretreatment.

Nitrogen adsorption and desorption isotherms were obtained at -196 °C on a Micromeritics ASAP 2020 equipment. Before the analysis, samples were dried at 100 °C for 24 h in an oven and then treated in situ under vacuum at 300 °C. The surface area was calculated using the Brunauer-Emmet-Teller (BET) equation based on the nitrogen adsorption isotherm in the pressure range of $0.05 \leq P/P_0 \leq 0.3$.[37]

The chemical composition of commercial samples was determined by X-ray fluorescence spectrometry (XRF) on a Bruker S8 Tiger instrument with a rhodium tube operating at 4 kW. Samples were analyzed without pretreatment using a semi-quantitative scanning method (QUANT-EXPRES / Bruker).

Temperature-programmed desorption of CO_2 (TPD-CO_2) was performed to characterize the surface base sites of the catalysts. Analyses were carried out on a multipurpose homemade apparatus coupled with an Omnistar QMS200 quadrupole mass spectrometer from Balzers. Solids (around 0.3 g) were pretreated in situ at 500 °C under a flow of 20 vol%

O_2/He at 30 mL.min^{-1} for 30 min. Afterwards, the reactor was cooled to room temperature, and CO_2 adsorption was performed for 1 h under a flow of CO_2 (15 mL.min^{-1}). Next, the reactor was purged with He at 30 mL.min^{-1}, and the desorption was carried out by heating the sample to 500 °C at a rate of 20 °C.min^{-1}. CO_2 desorption profiles were obtained based on the signal at m/z = 44. For calibration and quantitative measurements, pulses of pure CO_2 were analyzed before the main experiment. Experimental curves were mathematically deconvoluted using multiple Gaussian shaped peaks.[38] Each peak position was set from an initial estimative, and the calculations were conducted based on a nonlinear curve to minimize the deviations of the squares. Base sites were categorized as weak sites with desorption temperatures below 170 °C, medium sites with desorption temperatures ranging between 170 and 300 °C, and strong sites with desorption temperatures above 300 °C.

Surface acid sites were determined by temperature-programmed desorption of NH_3 (TPD-NH_3) using a multipurpose homemade apparatus equipped with a TCD detector. Samples (around 0.3 g) were pretreated in situ at 500 °C under a flow of 21% O_2/N_2 (vol%) at 30 mL.min^{-1} for 30 min. Sequentially, the reactor temperature was reduced to 100 °C, and the gas flow was switched to a mixture of 4 vol% NH_3/He to adsorb the probe molecule. The system was purged with He before NH_3 desorption, which was finally conducted by heating the samples under He flow (30 mL.min^{-1}) to 500 °C at a rate of 20 °C.min^{-1}. The calibration was also performed before analysis to allow for quantitative measurements. It was carried out by admitting pulses of 4% NH_3/He. Acid sites with desorption temperatures below 200 °C are categorized as weak, sites with desorption temperatures between 200 and 400 °C are considered medium acid sites, and sites with desorption temperatures above 400 °C are considered strong acid sites.

Thermogravimetric analysis were performed on post reaction catalysts on a NETZSCH STA 409 Pc Luxx. The samples were heated up to 600 °C at a rate of 20 °C.min^{-1} under synthetic air stream (30 mL.min^{-1}).

Catalytic reactivity tests

Catalytic conversion of pyruvaldehyde was studied in a fixed bed up-flow reactor (1/4 in Swagelok 316 stainless steel tube). To keep the catalyst bed in place, quartz wool was used in both ends of the reactor. The reactor temperature was varied between 100 and 180 °C, and the pressure was set at 30 bar using an Equilibar EB1LF2 back pressure regulator with a PTFE/glass diaphragm. A 0.2 mol.L^{-1} pyruvaldehyde aqueous solution was pumped by an Agilent 1100 Series HPLC pump at a flow rate of 0.2 mL.min^{-1}, following a space time of 3.5 min. The reaction products were collected periodically with the aid of a Valco selector valve and filtered using a 0.45 µm polypropylene membrane prior to analysis.

To determine any external mass transfer limitations, the flow rate was varied at constant space-time. To evaluate any effect from pore diffusion limitations, the catalyst particle size was varied from 53-63 µm to 90-100 µm. All tests were performed at different temperatures within 100-130 °C.

All aliquots were analyzed by high performance liquid chromatography (HPLC) in an Agilent 1260 Infinity HPLC equipped with a refractive index detector (RID) and a UV detector. A Hi-Plex H column was used at 35 °C in isocratic elution mode with a 0.05 mol.L^{-1} H_2SO_4 solution as mobile phase at a flow rate of 0.4 mL.min^{-1}. RID temperature was kept at 50 °C and UV analyses were performed at 210 nm.

The pyruvaldehyde conversion (X_P) and lactic acid selectivity (S_{AL}) and yield (Y_{AL}) were determined by:

$$X_P = \frac{C_{P_0} - C_{P_f}}{C_{P_0}} \times 100$$

$$S_{AL} = \frac{C_{AL}}{C_{P_0} - C_{P_f}} \times 100$$

$$Y_{AL} = \frac{X_P}{100} \times S_{AL}$$

Where C_{P0} is the initial pyruvaldehyde concentration, C_{Pf} is the final pyruvaldehyde concentration (the concentration at the time aliquots were collected for HPLC analyses) and C_{AL} is lactic acid concentration at the time aliquots were collected for HPLC analyses.

Acknowledgements

The authors acknowledge the financial support from CNPq (Brazil), FAPERJ (Brazil) and Solvay International Visitor Fund (USA). The Renewable Bioproducts Institute (Georgia Institute of Technology, USA) is likewise thanked for permitting the use of their facilities. E.M.A. also acknowledges CAPES (Brazil) for the scholarship (Process 99999.000879/2015-00). Lisa Wiest is thanked for experimental support.

Keywords: pyruvic aldehyde • Cannizzaro reaction • flow reactor • basicity • acidity

[1] A. Mansouri, R. Rihani, A. N. Laoufi, M. Özkan, *Fuel* **2016**, 185, 612-621

[2] A. Doshi, S. Pascoe, L. Coglan, T. J. Rainey, *Renew. Sust. Energ. Rev.* **2016**, 64, 329-337.

[3] a) A.L. Ahmad, N. H. M. Yasin, C. J. C. Derek, J. K. Lim, *Renew. Sust. Energ. Rev.* **2011**, 15, 584-593; b) A. E, Atabani, A. S. Silitonga, I. A. Badruddin, T. M I. Mahlia, H. H. Masjuki, S. Mekhilef, *Renew. Sust. Energ. Rev.* **2012**, 16, 2070-2093..

[4] N. Rahmat, A. Z. Abdullah, A. R. Mohamed, *Renew. Sust. Energ. Rev.* **2010**, 14, 987-1000.

[5] A. Villa, N. Dimitratos, C. E. Chan-Thaw, C. Hammond, L. Prati, G. J. Hutchings, *Accounts Chem Res* **2015**, 48, 1403-1412.

[6] Y. Li, M. Nielsen, B. Li, P. H. Dixneuf, H. Junge, M. Beller, *Green Chem.* **2015**, 17, 193-198.

[7] M. D. González, P. Salagre, R. Mokaya, Y. Cesteros, *Catal. Today* **2014**, 227, 171-178.

[8] P. Manjunathan, S. P. Maradur, A. B. Halgeri, G. H. Shanbhag, *J. Mol. Catal. A-Chem.* **2015**, 396, 47-54.

[9] H. R. Safaei, M. Shekouhy, S. Rahmanpur, A. Shirinfeshan, *Green Chem.* **2012**, 14, 1696-1704.

[10] a) M. Dusselier, P. Van Wouwe, A. Dewaele, E. Makshina, B. F. Sels, *Energy Environ. Sci.* **2013**, 6, 1415-1442; b) M. G. Manas, J. Campos, L. S. Sharninghausen, E. Lin, R. H. Crabtree, *Green Chem.* **2015**, 17, 594-600; c) M. Probst, J. Walde, T. Pümpel, A. O. Wagner, I. Schneider, H. Insam, *Appl. Microbiol. Technol.* **2015**, 99, 3029-3040.

[11] P. Mäki-Arvela, I. L. Simakova, T. Salmi, D. Y. Murzin, *Chem. Rev.* **2014**, 114, 1909-1971.

[12] a) H. Kishida, F. M. Jin, Z. Y. Zhou, T. Moriya, H. Enomoto, *Chem. Lett.* **2005**, 34, 1560-1561; b) Z. Shen, F. M. Jin, Y. L. Zhang, B. Wu, A. Kishita, K. Tohji, H. Kishida, *Ind. Eng. Chem. Res.* **2009**, 48, 8920-8925.

[13] Y. Shen, S. Zhang, H. Li, Y. Ren, H. Liu, *Chem-Eur J.* **2010**, 16, 7368-7371.

[14] A. K. Kinage, P. P. Upare, P. Kasinathan, Y. K. Hwang, J. S. Chang, *Catal. Commun.* **2010**, 11, 620-623.

[15] E. M. Albuquerque, L. E. P. Borges, M. A. Fraga, *J. Mol. Catal. A-Chem.* **2015**, 400, 64-70.

[16] E. M. Albuquerque, L. E. P. Borges, M. A. Fraga, *Green Chem.* **2015**, 17, 3889-3899.

[17] S. Bolado, R. E. TRevino, M. T. Garcia-Cubero, G. Gonzalez-Benito, *Catal. Commun.* **2010**, 12, 122-126.

[18] H. H. C. M. Pinxt, B. F. M. Kuster, G. B. Marin, *Appl. Catal. A-Gen.* **2000**, 191, 45-54.

[19] E. G. Rodigues, M. F. R. Pereira, J. J. Delgado, Z. Chen, J. J. M. Órfão, *Catal Commun.* **2011**, 16, 64-69; b) G. M. Lari, R. Garcia-Muelas, C. Mondelli, N. Lopez, J. Perez-Ramirez, *Green Chem.* **2016**, 18, 4682-4692.

[20] S. Lux, M. Siebenhofer, *Catal. Sci. Technol.* **2013**, 3, 1380-1385.

[21] a) M. J. Antal, W. S. L. Mok, G. N. Richards, *Carbohyd. Res.* **1990**, 199, 111-115; b) Y. Koito, K. Nakajima, M. Kitano, M. Hara, *Chem. Lett.* **2013**, 42, 873-875.

[22] C.G. Swain, A. L. Powell, W. A. Sheppard, C. R. Morgan, *J. Am. Chem. Soc.* **1979**, 101, 3576-3583.

[23] C. Sievers, Y. Noda, L. Qi, E. M. Albuquerque, R. M. Rioux, S. L. Scott, *ACS Catal.* **2016**, 6, 8286-8307.

[24] L. Yang, J. Su, S. Carl, J. G. Lynam, X. Yang, H. Lin, *Appl. Catal. B-Environ.* **2015**, 162, 149-157.

[25] E. Fernandez Lopez, V. Sanchez Escribano, M. Panizza, M. M. Carnasciali, G. Busca, *J. Mater. Chem.* **2001**, 11, 1891-1897.

[26] P. Bouvier, E. Djurado, C. Ritter, A. J. Dianoux, G. Lucanzeau, *Int. J. Inorg. Mater.* **2001**, 3, 647-654.

[27] a) H. C. Choi, Y. M. Jung, S. B. Kim, *Vib. Spectrosc.* **2005**, 37, 33-38; b) V. Swamy, A. Kuznetsov, L. S. Dubrovinsky, R. A. Caruso, D. G. Shchukin, B. C. Muddle, *Phys. Rev. B* **2005**, 71, 184302.

[28] M. Thommes, K. Kaneko, A. V. Neimark, J. P. Olivier, F. Rodriguez-Reinoso, J. Rouquerol, K. S. W. Sing, *Pure Appl. Chem.* **2015**, 87, 1051-1069.

[29] a) S. Kouva, K. Honkala, L. Lefferts, J. Kanervo, *Catal. Sci. Technol.* **2015**, 5, 3473-3490; b) G.-Y. Yang, Y.-H. Ke, H.-F. Ren, C.-L. Liu, R.-Z. Yang, W.-S. Dong, *Chem. Eng. J.* **2016**, 283, 759-767; c) Y. Zhao, W. Li, M. Zhang, K. Tao, *Catal. Commun.* **2002**, 3, 239-245.

[30] a) C. N. Chervin, B. J. Clapsaddle, H. W. Chiu, A. E. Gash, J. H. Satcher, S. M. Kauzlarich, *Chem. Mater* **2005**, 17, 3345-3351; b) F. Gallino, C. Di Valentin, G. Pacchioni, *Phys. Chem. Chem. Phys.* **2011**, 13, 17667-17675; c) J. P. Goff, W. Hayes, S. Hull, M. T. Hutchings, K. N. Clausen, *Phys. Rev. B* **1999**, 59, 14202-14219.

[31] C. A. Franchini, A. M. Duarte de Farias, E. M. Albuquerque, R, dos Santos, M. A. Fraga, *Appl. Catal. B-Environ.* **2012**, 117-118, 302-309.

[32] K.-H. Jacob, E. Knozinger, S. Benier, *J. Mater. Chem.* **1993**, 3, 651-657.

[33] a) V. Bolis, C. Morterra, M. Volante, L. Orio, B. Fubini, *Langmuir* **1990**, 6, 695-701; b) C. Morierra, R. Aschieri, M. Volante, *Mater. Chem. Phys.* **1988**, 20, 539-557.

[34] N. Dinitratros, J. A. Lopez-Sanchez, S. Meenakshisundaram, J. M. Anthonykutty, G. Brett, A. F. Carley, S. H. Taylor, D. W. Knight, G. J. Hutchings, *Green Chem.* **2009**, 11, 1209-1216.

[35] J. L. Xu, H. Y. Zhang, Y. F. Zhao, B. Yu, S. Chen, Y. B. Li, L. D. Hao, Z. M. Liu, *Green Chem.* **2013**, 15, 1520-1525.

[36] A. Saadi, Z. Rassoul, M. M. Bettahar, *J. Mol. Catal. A-Chem.* **2006**, 258, 59-67.

[37] K. S. W. Sing, D. H. Everett, R. A. W. Haul, L. Moscou, R. A. Pierotti, J. Rouqueroul, T. Siemieniewska in *Handbook of Heterogeneous Catalysis*, Vol. 2, Wiley-VCH, Weinheim, **2008**, pp. 1222-1224.

[38] A. O. Menezes, P. S. Silva, E. P. Hernandez, L. E. P. Borges, M. A. Fraga, *Langmuir* **2010**, 26, 3382-3387.

10.1002/cctc.201700305

WILEY-VCH

Entry for the Table of Contents (Please choose one layout)

Layout 2:

FULL PAPER

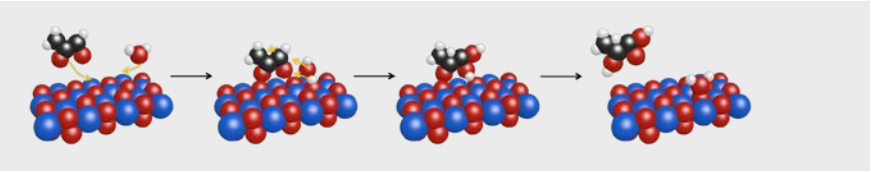

Lewis acid sites and mobile surface hydroxyl groups play significant roles in the Cannizzaro reaction of pyruvaldehyde over ZrO_2-based catalysts.

Elise M. Albuquerque, Luiz E. P. Borges, Marco A. Fraga, Carsten Sievers**

Page No. – Page No.

Relationship between acid-base properties and the activity of ZrO_2 catalysts for the Cannizzaro reaction of pyruvaldehyde to lactic acid

10.1002/cctc.201700305